The Trigger System of the NOMAD Experiment

J. Altegoer[1], J. Andrle[1], S. Boyd[2], A. Cardini[3,4], P. Farthouat[5], R. Ferrari[6], D. Geppert[1],
C. Gößling[1], W. Huta[5], N. Hyett[7], N. Koch[1], A. Lanza[6], J. Long[8,9], G.F. Moorhead[7],
D. Pollmann[1], C. Poulsen[7], A. Rubbia[10], B. Schmidt[1,5], F.J.P. Soler[2,5], D. Steele[8,11],
K.E. Varvell[2,12], T. Weiße[1], L.J. Winton[7], B.D. Yabsley[2] and A. Voullieme[1].

Abstract

The NOMAD trigger system is described in the present paper. It is made up of a large area plastic scintillator veto system, two trigger scintillator planes inside a 0.4 T magnetic field and their associated trigger electronics. Special features of the system consist of the use of proximity mesh photomultipliers which allow the trigger scintillators to operate in the magnetic field, and the use of custom-built VME modules which perform the trigger logic decisions, the signal synchronisation and gate generation, event counting and livetime calculations. This paper also includes a description of each of the NOMAD triggers, with their calculated and measured rates, efficiencies and livetimes.

[1]Dortmund Univ., Dortmund, Germany.
[2]Univ. of Sydney, Sydney, Australia.
[3]UCLA, Los Angeles, California, USA.
[4]Now at INFN Roma, Univ. of Roma "La Sapienza", Rome, Italy.
[5]CERN, Geneva, Switzerland.
[6]Univ. of Pavia and INFN, Pavia, Italy.
[7]Univ. of Melbourne, Melbourne, Australia.
[8]Johns Hopkins Univ., Baltimore, MD, USA.
[9]Now at Univ. of Colorado, Boulder, CO, USA.
[10]ETH Zürich, Zürich, Switzerland, on leave from CERN.
[11]Now at Univ. of Lausanne, Lausanne, Switzerland.
[12]ANSTO Sydney, Menai, Australia.

1 Introduction

The NOMAD (Neutrino Oscillation Magnetic Detector) experiment is a short baseline appearance search for $\nu_\mu \rightarrow \nu_\tau$ oscillations at the CERN West Area Neutrino Facility (WANF) running at the SPS (Super Proton Synchroton) accelerator. The aim of the experiment is to identify a potential ν_τ charged current (CC) interaction by the kinematical signatures associated with the observation of either a leptonic or hadronic decay of the τ^- inside NOMAD. First limits on $\nu_\mu \rightarrow \nu_\tau$ oscillations have already been set by the experiment with an analysis of the data collected during 1995 [1] and preliminary limits have been set with the data collected until 1997 [2].

NOMAD consists of an active target of drift chambers embedded inside a 0.4 T dipole magnetic field occupying a volume of $7.5 \times 3.5 \times 3.5$ m^3. The drift chambers serve the double purpose of providing a target for the neutrino interactions and performing the tracking of all charged particles. These are followed by a transition radiation detector (TRD) for electron identification, a preshower, an electromagnetic calorimeter, and two planes of trigger scintillators also inside the magnet. Upstream of the magnet is a veto system and a front calorimeter installed in the front iron support, while a hadronic calorimeter and a set of muon chambers lie downstream of the magnet (see Fig. 1). A general overview of the NOMAD detector and its characteristics can be found in [3]. In addition to $\nu_\mu \rightarrow \nu_\tau$ oscillations, NOMAD is also sensitive to $\nu_\mu \rightarrow \nu_e$ oscillations [4] and other neutrino physics topics (see [5] for an example).
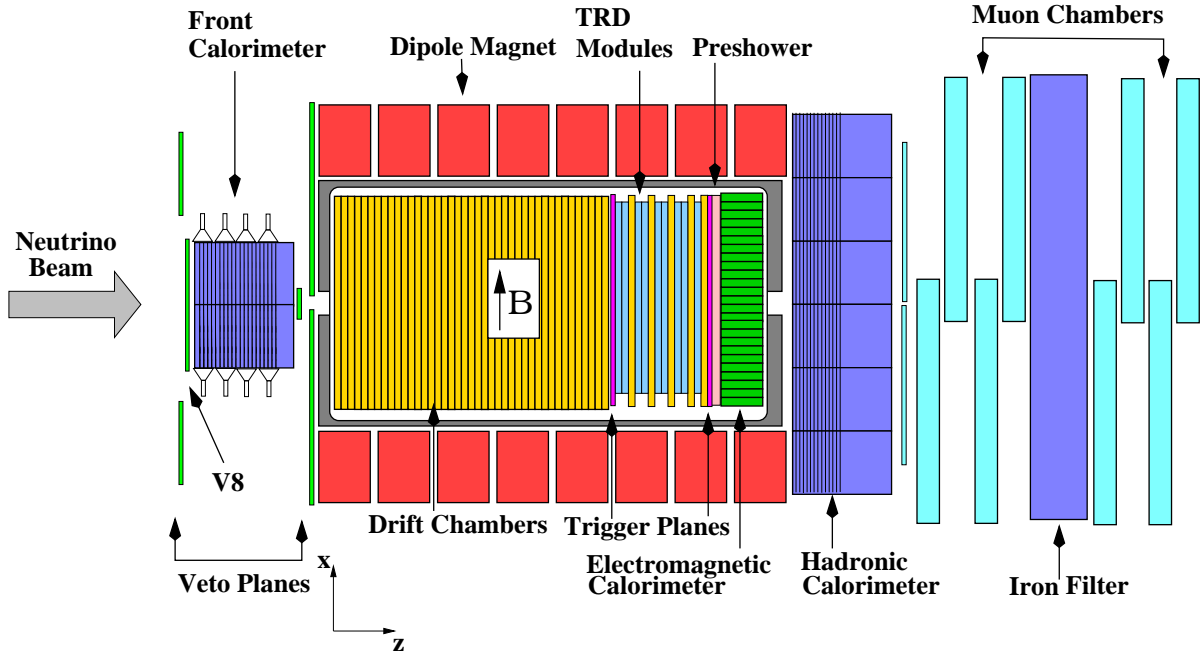

Figure 1: A top view of the NOMAD detector.

The present paper describes the trigger system of the NOMAD experiment. It consists of an array of veto scintillators upstream of the main target (described in section 2), two planes of trigger scintillators inside the magnet (section 3)

and dedicated VME trigger modules MOTRINO (Modular Trigger for NOMAD) which perform the trigger logic for the whole experiment (section 4). The measured and calculated rates, efficiency and livetimes associated with each of the NOMAD triggers (section 5) completes the description of the trigger system.

2　Veto Scintillators

The veto system of the NOMAD experiment is an array of 59 scintillation counters [6] covering an area of 5.4×5.0 m^2 upstream of the NOMAD target. The aim of the veto is to prevent muons associated with the neutrino beam (the "muon-halo"), other charged particles from interactions upstream of NOMAD, or cosmic rays in coincidence with the neutrino burst, which cross the detector, from producing valid triggers.

2.1　Layout

The veto was separated into 9 distinct groups (or banks) built around the front support for the magnet (which also contains the front calorimeter, see Figs. 1 and 2). Due to the presence of the support beam for the steel structure in which the central detector is mounted (the "basket"), a small fraction of interactions in part of this front support and in the magnet coil cannot be vetoed and have to be identified by the reconstruction of the event vertex.

The NE-110 scintillators[1] are 2 cm thick, 21 cm wide and come in two lengths: 210 cm and 300 cm. There are 56 of them that are viewed on both ends by Philips XP-2020 photomultipliers, with the remainder (3) having single-ended readout due to lack of space between the iron support and the magnet flux return. The stray magnetic fields are less than 200 Gauss, so mu-metal covers are sufficient to provide effective shielding.

For long scintillators of 300 cm, the transit time difference between the passage of particles transiting at different points along the length of the counter results in unacceptable timing jitter. For this reason, mean-timer modules manufactured at Padova University [7] providing an output signal which does not depend on the position at which the particle traversed the counter were used in the electronics. The two photomultiplier outputs from each double-ended scintillator are fed via nine discriminators (LeCroy 4413, set at 25 mV) to the inputs of nine mean-timer modules. A single module can take up to 8 pairs of discriminated signals and produces two sets of 8 outputs. A valid output has a delay of 40 ns and is produced if the two signals from a pair have at least a 40 ns overlap. The mean-timer outputs are then fed into a LeCroy 1876 96-channel Fastbus time to digital converter (TDC) module with a resolution of 1 ns. Each mean-timer module also produces a single output consisting of the logical OR of all eight output signals, with the OR from eight of the mean-timer modules making up the combined veto signal (see Fig. 3). This signal has been set to have a width of 100 ns. Six counters, those mounted on the upper-left and upper-right of the magnet flux return iron, lie outside the acceptance of the trigger planes and are
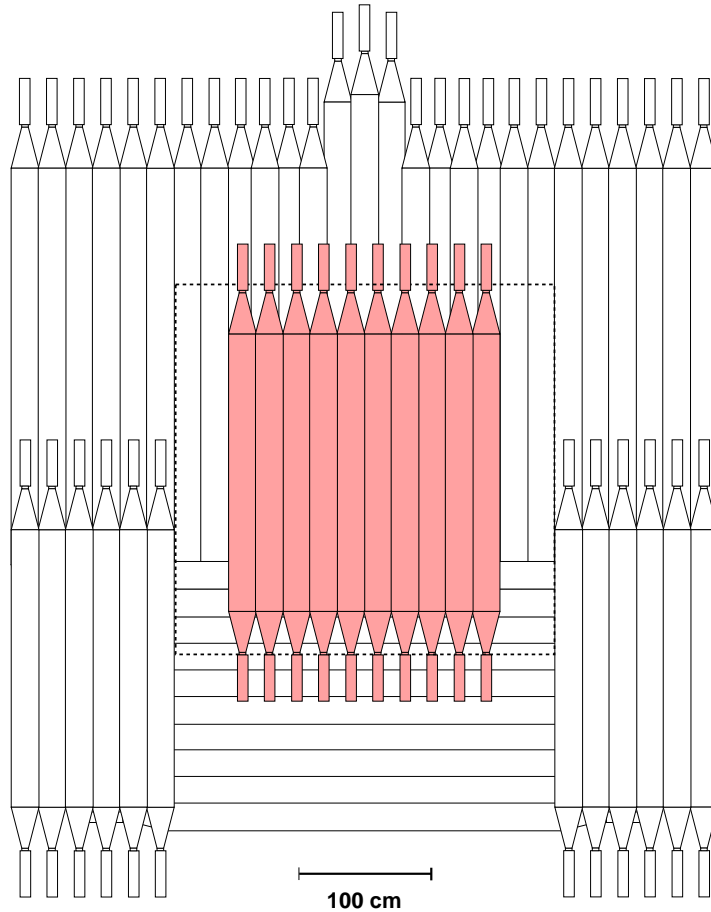
---

[1]Manufactured by Nuclear Enterprises, UK.

Figure 2: Front view of the NOMAD veto. The shaded area is the central veto bank called V_8. The dotted line is the sensitive drift chamber volume.

excluded from the OR in order to reduce deadtime. For triggers occurring in the front calorimeter, the veto is formed by the OR of the 10 counters in bank 8 (designated V_8, the shaded area of Fig. 2) which is situated upstream of the front face of the support.

The SPS cycle of 14.4 s consists of two neutrino spills of 4 ms duration (fast/slow extraction) separated by 2.6 s, with a 2.0 s "flat-top" slow extraction (the muon gate) between them. The particles from the muon gate originate from test beams in the West Area of the SPS upstream of NOMAD and are used by NOMAD for calibration and alignment purposes. The adjustment of the photomultiplier high voltages was performed with muons in the "flat-top". A small trigger scintillator was placed on the opposite end of the scintillator from the photomultiplier to be calibrated. Using a pulse height analyser, the total charge collected from the scintillator and its equivalent pulse height (in millivolts) were recorded when a muon traversed the scintillator at the opposite end of its length. The high voltage of the photomultiplier was varied until the peak of the pulse height distribution was at 100 mV, four times the threshold value of 25 mV. This procedure, repeated for all 115 photomultiplier tubes, enabled veto signals to be obtained even when a particle traversed a scintillator at one of the extremes where the attenuation is highest.
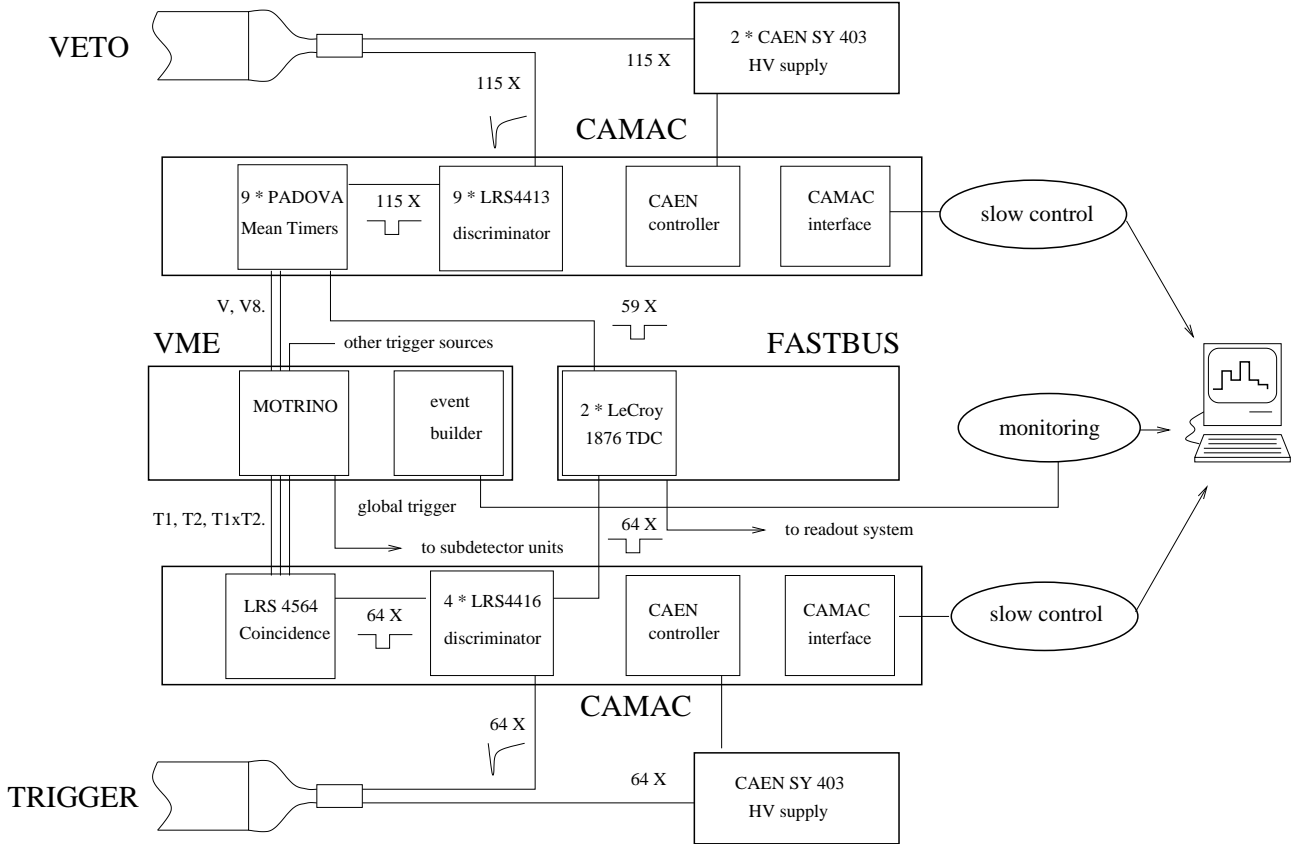
3

Figure 3: Schematic of the electronics for the veto and the trigger.

Cosmic rays in coincidence with the neutrino spill but travelling in the direction opposite to the beam (in which case the trigger scintillators fire before the veto) are vetoed by arranging that the signals from the banks whose average height are below those of the trigger have signals that arrive 25 ns earlier than those from the other banks.

The high voltages and currents of each photomultiplier in the veto, and the threshold levels of each discriminator are controlled by means of a slow control program written in the graphics–based language LabVIEW [8]. These are constantly being checked against their nominal values, and alarms are generated if the values lie outside a specified range. A monitoring program also generates summary histograms of the veto TDC.

2.2 Performance

The efficiency of the veto has been monitored on a cycle by cycle basis throughout the NOMAD data taking period (1995 to 1998) with the aid of the spectrometer of the CHORUS experiment [9], the $\nu_\mu \rightarrow \nu_\tau$ oscillation experiment upstream of NOMAD. Muons crossing the CHORUS spectrometer (C) in coincidence with the two trigger planes (T_1 and T_2) of NOMAD were used to check whether the veto (V) fired or not. The ratio of the number of CVT_1T_2 coincidences with respect to CT_1T_2 was a measure of the veto efficiency. These values are recorded in Table 1. The increases in efficiency in the 1996 and 1997 runs are due to

4

Year	V	T_1	T_2	$T_1 \times T_2$
1995	95.2 ± 0.1	98.0 ± 0.1	95.0 ± 0.2	93.5 ± 0.2
1996	96.5 ± 0.1	99.1 ± 0.1	96.1 ± 0.1	95.3 ± 0.1
1997	97.8 ± 0.1	99.1 ± 0.1	95.8 ± 0.1	95.0 ± 0.1
1998	97.8 ± 0.1	99.3 ± 0.1	96.4 ± 0.1	95.8 ± 0.2

Table 1: Single track efficiencies for the veto and trigger planes.

improvements in individual counters after each year.

The veto fires at a rate of (790 ± 140) per 10^{13} protons on target (p.o.t.) depending on the beam conditions, which is equivalent to a muon rate of (29 ± 5) m^{-2} per 10^{13} p.o.t. Since the pulse width is 100 ns, this introduces a dead-time of the order of 4% into the normal trigger configuration flagging a neutrino interaction inside the drift chamber target for which the two trigger planes fire and the veto does not $(\overline{V} \times T_1 \times T_2)$.

3   The Trigger Hodoscopes

NOMAD contains two planes of trigger scintillators (T_1 and T_2) inside the magnet. The first plane follows the active target and the second plane is positioned behind the TRD region. Both planes cover a fiducial area of 280×286 cm^2 and consist of 32 scintillation counters, as shown in Fig. 4, with single-ended readout. The scintillators have a thickness of 0.5 cm and a width of 19.9 cm. In each plane, 28 counters of length 124 cm are installed horizontally and 4 counters of length 130 cm are installed vertically to cover the adiabatic lightguides of the horizontal counters. The lightguides of the vertical counters are bent by 90° because the photomultipliers can only be operated parallel to the magnetic field.

3.1   Trigger Scintillators

The scintillator used is a fast (less than 2.1 ns) BC-408 premium organic plastic scintillator produced by the Bicron Corporation [10]. The propagation of the scintillation light in the counters was investigated using a fast digital oscilloscope interfaced to a personal computer.

Measurements of both the pulse height and the integrated charge at various distances x from the readout face are shown in Fig. 5. A minimum is observed in the pulse height distribution due to the difference in arrival times of the direct and reflected components of the light. Due to the excellent time resolution of the scintillator and photomultiplier tube (PMT, see section 3.2), the direct and the reflected signal (which is attenuated with respect to the direct one) can be separated when they are produced close to the PMT. When the signal is at the opposite end of the PMT, the two signals can no longer be resolved and they both add up, giving a large pulse height. A minimum is observed when the signals originate in the centre of the scintillator. The attenuation length determined from the direct component ($x < 60$ cm) can be extracted from a simple exponential fit, and was found to be $\lambda = (143 \pm 2)$ cm.
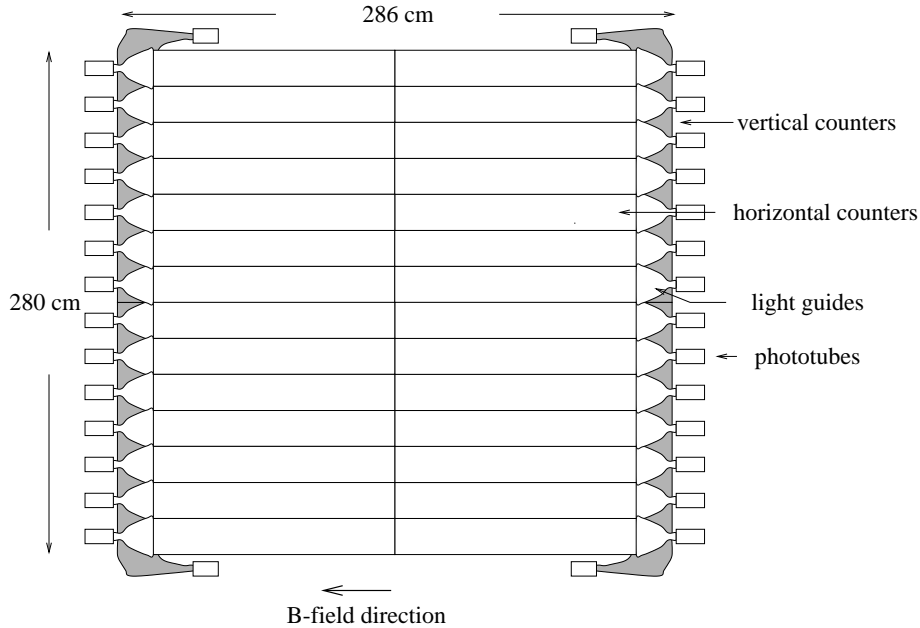
Figure 4: Layout of the trigger planes T_1 and T_2. The four vertical scintillation counters are shaded.

The effect is completely different when the PMT is operated in charge integrating (or calorimetric) mode, where both the direct and reflected components contribute to the total charge. The signal is the lowest at the farthest end of the scintillator (rather than at the centre). There seems to be some evidence of the signal falling rapidly below 30 cm, with an attenuation length comparable to the one determined from the direct component of the light, and more slowly from 30 to 120 cm.

Because of the necessity for fast triggering, these counters were operated in pulse height mode. The reflections from the far end ensured that the signal was always more than 70% of the maximum pulse height found close to the photomultiplier.

3.2 Trigger Photomultipliers

The use of conventional phototubes with magnetic shielding inside an environmental field of 0.4 T cannot provide a satisfactory detection efficiency, since the long paths from the photocathode to the first dynode result in a deflection of the electrons from their normal trajectories and therefore in a loss of gain.

Phototubes that utilize transmission mesh dynodes of non-magnetic material [12, 13] have been succesfully operated in strong magnetic fields. These dynodes are aligned axially, parallel to each other, thus requiring no electrostatic focusing system to guide the electrons. These PMTs work well in magnetic fields, provided that the mesh is sufficiently thin so that the deformation of secondary electron orbits is negligible [12] and that the axis of the photomultiplier is parallel to the magnetic field. HAMAMATSU type R-2490-05 [14] photomultiplier tubes with 16 dynodes of proximity mesh and a bialkali photocathode of 1.5 inch in diameter were chosen for the trigger scintillators of the NOMAD experiment because of
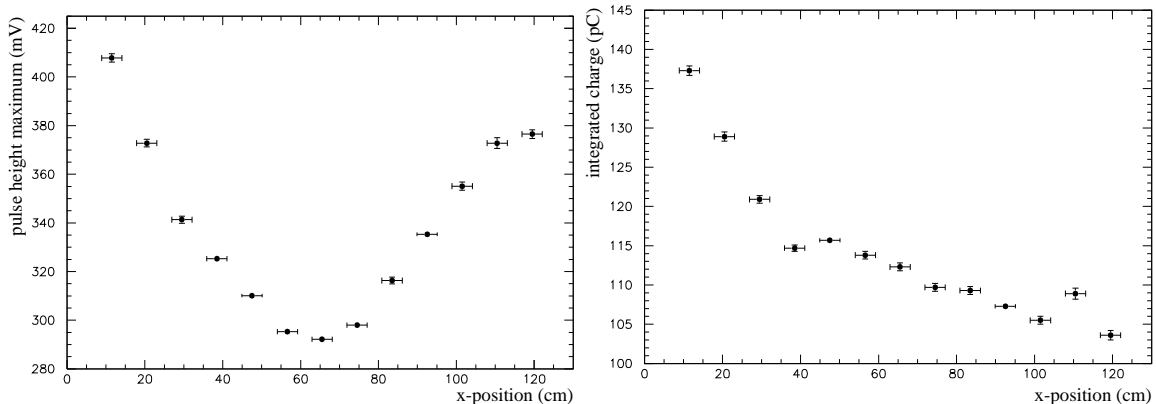
6

Figure 5: Maxima of pulse height and integrated charge of minimum ionizing particles traversing the scintillator as a function of x [11].

their high gain (necessary because the scintillators are only 0.5 cm thick), their small physical size and relatively low cost.

The number of photoelectrons for a minimum ionizing particle (N_e^{mip}) was determined from the charge collected Q_{mip} and by comparing to the signals obtained from a pulsed LED (type XP21) with very stable light output (in which the contribution of the LED-noise to the photostatistics is negligible) and maximum wavelength of emission of 630 nm. The photoelectron number for the LED pulser N_e^{LED} was calculated from the fluctuations in the anode distribution under the assumption of Poisson statistics broadened by the fluctuations in the dynode chain [15]:

$$N_e^{LED} = \left(\frac{Q_{LED}}{\sigma_Q}\right)^2 \left[1 + \frac{1}{g_1} + \frac{1}{g_1(g-1)}\right] , \tag{1}$$

where Q_{LED} is the mean of the total charge distribution for the LED, σ_Q is the standard deviation, $g_1 \sim 5.2$ is the gain of the first dynode and $g \sim 2.6$ is the average gain of subsequent dynodes. Assuming response linearity, the photoelectron number for a minimum ionizing particle is on average:

$$N_e^{mip} = N_e^{LED}\frac{Q_{mip}}{Q_{LED}} = 83 \pm 7 ,$$

which allows a good signal detection efficiency.

The absolute gain of the photomultipliers, defined as the ratio of the number of electrons collected at the anode to the number of photoelectrons from the photocathode, has been studied as a function of the supply voltage (Fig. 6(a)). At around 2200 V (80% of the maximum voltage allowed) an average gain of 1.1×10^7 was achieved. The final working voltage of the phototubes was determined by using muons in the "flat-top" with a coincidence between a counter in the first plane with the corresponding counter in the same position in the second plane. The high voltage of each photomultiplier tube was set such that the pulse height of minimum ionizing particles with a magnetic field of 0.4 T was ~ 400 mV.

The noise rate of the photomultiplier tube stabilises around 50 s^{-1} above 50 mV discriminator threshold (see Fig. 7(a)). The rate of muon triggers per 10^{13} p.o.t. was measured as a function of the discriminator threshold and it was
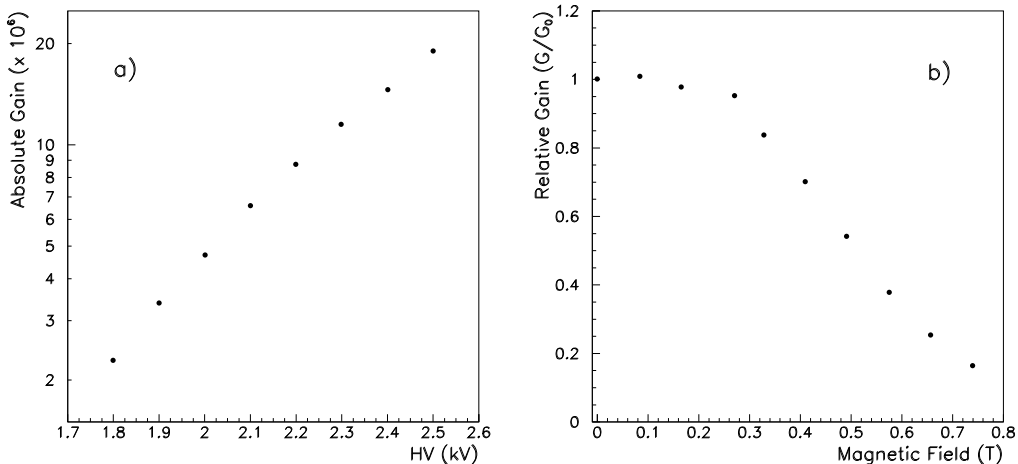
Figure 6: (a) The absolute gain at different supply voltages for an example PMT and (b) relative gain G/G_0 for the same PMT in a magnetic field.

found that the rate started diminishing significantly above 100 mV (see Fig. 7(b)). The discriminator threshold was set at 50 mV to obtain maximum efficiency.

In order to determine the photomultiplier response under the influence of a magnetic field, a test photomultiplier was placed parallel to the uniform field of a dipole magnet and illuminated by the high quality LED mentioned above. The relative gain G/G_0 of the phototube as a function of the magnetic field is shown in Fig. 6(b). With a field of 0.4 T the response is still 70% of the nominal value[2]. The signal resolution σ_Q/Q as a function of magnetic field remains very stable: $\sigma_Q/Q = (17 \pm 2)\%$ from 0 to 0.8 T. The response of a large sample of the phototubes has been measured after the setup of the trigger planes in NOMAD. The average value for the relative gain was found to be 74%.

The time response of a trigger counter was measured with a betatron at the University of Dortmund. A timing precision of ~ 800 ps and an effective signal propagation velocity of 13 cm/ns (consistent with the speed of light in the scintillators, if the reflections of the light on the counter surface are taken into account) were measured. The jitter in the timing distribution obtained from the trigger planes is ~ 3 ns (due to signal propagation in the scintillators). This time stamp is the reference timing signal that is used as seed for the reconstruction of tracks in the NOMAD drift chambers.

Problems encountered during the operation of these phototubes were the occasional breakdown of resistors in the base and damage to discriminator inputs. These were attributed to the same cause: sparking in the phototube causing high voltage spikes in the voltage divider. This effect has been also observed by the SpaCal group of the H1 experiment [18] where they deduced that it was due to field emission discharges from the sharp edges of the thin metal rods which

---

[2]The relative response of phototubes with a small number of transmission dynodes is even better [16]. However, triodes or tetrodes can only be used in situations where the particles deposit sufficient visible energy in the active detector material, for instance in homogeneous calorimeters like the NOMAD electromagnetic calorimeter [17].
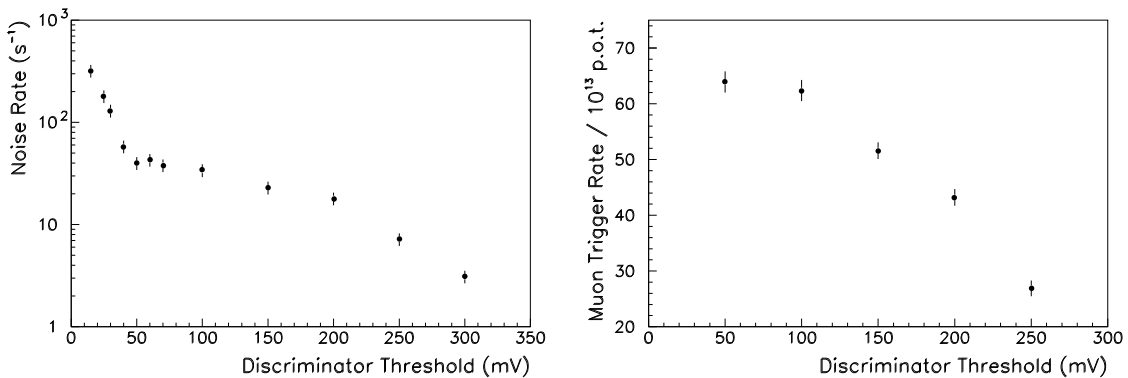
Figure 7: (a)Noise rate of a photomultiplier as a function of the discriminator threshold. (b)Muon trigger rate per 10^{13} p.o.t. as a function of the discriminator threshold.

connect the dynode grids. The solution to this problem was the introduction of a 1 MΩ resistor inside the voltage divider between the high voltage connector and the cathode to limit the signal size.

3.3 Trigger Electronics

The electronic chain for the trigger counters is shown schematically in Fig. 3. The 64 analog signals of the individual counters are first discriminated, using four programmable LeCroy 4416 units, which provide two ECL logic outputs of 40 ns width for each of the counters.

One of the discriminator ECL signals is sent to a TDC (LeCroy 1876) that records it to tape, while the other output is sent to a 64 channel OR-logic unit (LeCroy 4564), which performs logical combinations between the four groups of 16 input ORs. This unit provides the T_1 and T_2 signals which are the logical OR of the 32 counters in each plane, and the $T_1 \times T_2$ signal, which is the logical AND between the two planes.

The voltages and currents of the photomultipliers and the discriminator thresholds are checked constantly by means of a slow control program written in Lab-VIEW [8] as in the case of the veto. Any slow control data which is out of range causes an alarm which is sent to the central data acquisition. A monitoring program connected to the trigger generates summary histograms of the recorded subdetector data.

3.4 Trigger counter efficiencies

The detection efficiency of minimum ionizing particles for the 64 trigger counters has been determined using muons from dedicated triggers not incorporating T_1 or T_2 (see section 5). Reconstructed muon tracks have been extrapolated to the scintillation counters and compared with the data recorded in the trigger TDC, rejecting events close to the edges. For tracks where the distance from the reconstructed track to the edge of the scintillator was smaller than 5 mm, the

9

trigger counter efficiency dropped due to alignment uncertainties and multiple scattering. The average efficiency for minimum ionizing particles traversing the counters in T_1 is $(98.1 \pm 0.1)\%$ and those in T_2 is $(96.0 \pm 0.2)\%$, the difference due to individual counters in each plane.

In order to obtain the global efficiencies of the planes, the geometrical acceptance due to small gaps (≤ 1 mm) between the scintillators has to be taken into account as well as the counter inefficiency described above. By studying the position of extrapolated muon tracks to the two trigger planes which had no hits in T_1 or T_2, it was determined that the global inefficiency is dominated by the inefficiencies in individual counters. Only a small contribution of the geometrical acceptance to the global inefficiency was visible in the centre region where the two sets of horizontal scintillators meet in plane 2. The measured efficiencies are summarized in Table 1.

It should be noted that the efficiencies given for the coincidence $T_1 \times T_2$ are for single tracks. For neutrino interactions with two or more tracks, which is the normal case, this efficiency increases to more than 99.6%. The implication of the single track efficiency on the different types of neutrino interactions in the drift chamber target will be discussed in section 5.

4   The MOTRINO Module

Compared to other high energy physics experiments, the trigger for a neutrino experiment seems very simple since the event rate is low and different trigger levels are not required. The speed of the trigger decision could be accommodated by conventional electronics used to perform coincidences between the trigger and veto signals. However, the system increases in complexity when several targets for neutrino interactions and different trigger types such as neutrino or muon triggers are used in conjunction with the beam cycle. A VME-based module called MOTRINO (MOdular TRIgger for NOmad) was designed and implemented within the NOMAD data aquisition system to provide computer controlled selection of triggers and to record information on trigger types and trigger inputs [19].

4.1   Overview

The data aquisition system of NOMAD centres around five local system crates (LSC), each of which is associated with a NOMAD subdetector, and an event builder (EVB) [3]. Each LSC can be operated in two different modes: in stand-alone mode (for debugging purposes) or as part of the global aquisition. In the first case local triggers have to be generated; the second one uses global triggers. The different configurations of the data aquisition require a MOTRINO board in the EVB as well as in each LSC. The boards can be operated in various modes and configurations:

- *Global master configuration*
  The trigger board in this configuration generates the physics triggers and

the time signals to synchronize datataking with the beam cycle. It receives Busy signals from the different LSC[3].

- *Global slave configuration*
  The cards in the slave configuration receive the trigger and the synchronisation gates from the master and send them to a Fastbus controller card which in turn transmits the physics gates and the trigger to the front-end electronics. The Busy signals of the corresponding subdetector are transmitted to the master.

- *Local master configuration*
  In this configuration the trigger card runs in stand-alone mode. It generates its own triggers and does not transmit the subdetector Busy.

- *Local slave configuration*
  This case is similar to the global slave configuration. The only difference is that the subdetector Busy is not transmitted to the master card.

4.2   Layout

The MOTRINO board is connected to a VME standard bus with a special connector for the supply of -5 V and -2 V. The modules in the different LSC and the EVB are connected to each other by an independent differential bus, which is used for the transmission of the physics gates and the trigger and Busy signals.

The board has eight inputs for trigger and veto signals. Up to six physics triggers, formed from programmable combinations of these inputs, are available on the front panel of the differential bus. Further LEMO connectors are used for a physics trigger input and a calibration trigger output in case of operation as slave card, a synchronization signal for the start of the SPS-cycle and an external clock for the measurement of the individual trigger livetimes. A flat cable links the MOTRINO card with the Fastbus controller board mentioned above. A LED status display indicates the mode of operation of the module.

A large number of the logic functions of MOTRINO are realized by programmable logic devices (PLDs). For trigger formation, a programmable array logic (GAL 22V10B) [20] is used which combines a high performance CMOS process with Electrically Erasable (E^2) floating gate technology.

The limited amount of space on the VME–board called for even more complex CMOS devices in order to implement the various logic functions. Most of the high-performance EEPROMs used are based on the Multiple Array Matrix architecture (ALTERA MAX 7000) [21], which was the fastest high-density programmable logic family available in 1995 when the card was designed. The largest implemented chip of this family provides 5000 usable gates and 256 macrocells.

4.3   Functionalities

The MOTRINO module performs various important tasks related to the triggering in the NOMAD experiment, which will be described in the following para-

---

[3]In order to increase the number of possible physics triggers, a second master configuration, which does not generate synchronisation signals, was introduced in 1996.

graphs (see also Fig. 8).

4.3.1 Gate Generation

The two 4 ms long neutrino gates separated by the 2.0 s "flat-top" muon gate are generated by MOTRINO with a precision of 8 μs and are synchronised with the SPS neutrino beam cycle. In order to provide the timing signals with high stability, the gate generation is based on the 16 MHz VME-clock. Between the physics gates, short time windows of several hundred microseconds are introduced to allow the readout of the frontend electronics. During the pause of 10.7 s between the second neutrino spill and a new cycle, up to eight additional gates (the calibration gates) can be generated in the MOTRINO slave boards, for which the master module provides the start signal.

4.3.2 Trigger Formation, Selection and Moderation

Up to six different trigger types can be formed from eight subdetector signals in each of the physics gates, using the GAL 22V10B. Since the propagation delay time of this GAL is only 7.5 ns, fast trigger formation is possible. Signals containing the various gates and the mask for a given trigger type can also be stored in a control register. This allows a computer controlled trigger selection.

In order to prevent two consecutive outputs very close in time before the Busy is enabled, the sequential logic of the GAL 22V10B is used. The output signal of a satisfied trigger condition is fed back to the input array of the GAL and acts as a fast inhibit. The (asynchronous) reset of the fast inhibit is caused by the beginning of the Busy signal from the readout electronics.

Additional deadtime (used in the muon gate to limit the number of events registered) can be introduced for the triggers by means of a stretcher signal, which is supplied to one of the I/O pins of the GAL. An eleven bit register is used to set the duration of the deadtime. The clock period is 2 μs during the neutrino gates and 2 ms during the muon gate.

The logical OR of the six trigger types represents the global event trigger which is sent to the frontend electronics via the slave boards in the LSC and the FASTBUS controller card during the two neutrino and the muon gates. The same functionalities are available for the formation of local triggers and for stand-alone operation during the calibration gates.

4.3.3 Livetime determination

An additional GAL 22V10B is used to provide coincidences of the various trigger inputs and the Busy signal with an external clock. Since the intensity of the neutrino beam is not uniform in time, an external signal ($SP5$) is used which reflects the structure of the beam[4]. The coincidence rates are necessary to determine the livetime of the individual triggers. For the case of the $\overline{V}T_1T_2$ trigger (see section

---

[4]The clock signal is generated by a scintillator positioned in the muon shield of the neutrino beam line which provides signals whose instantaneous frequency is proportional to the muon and hence the neutrino flux.
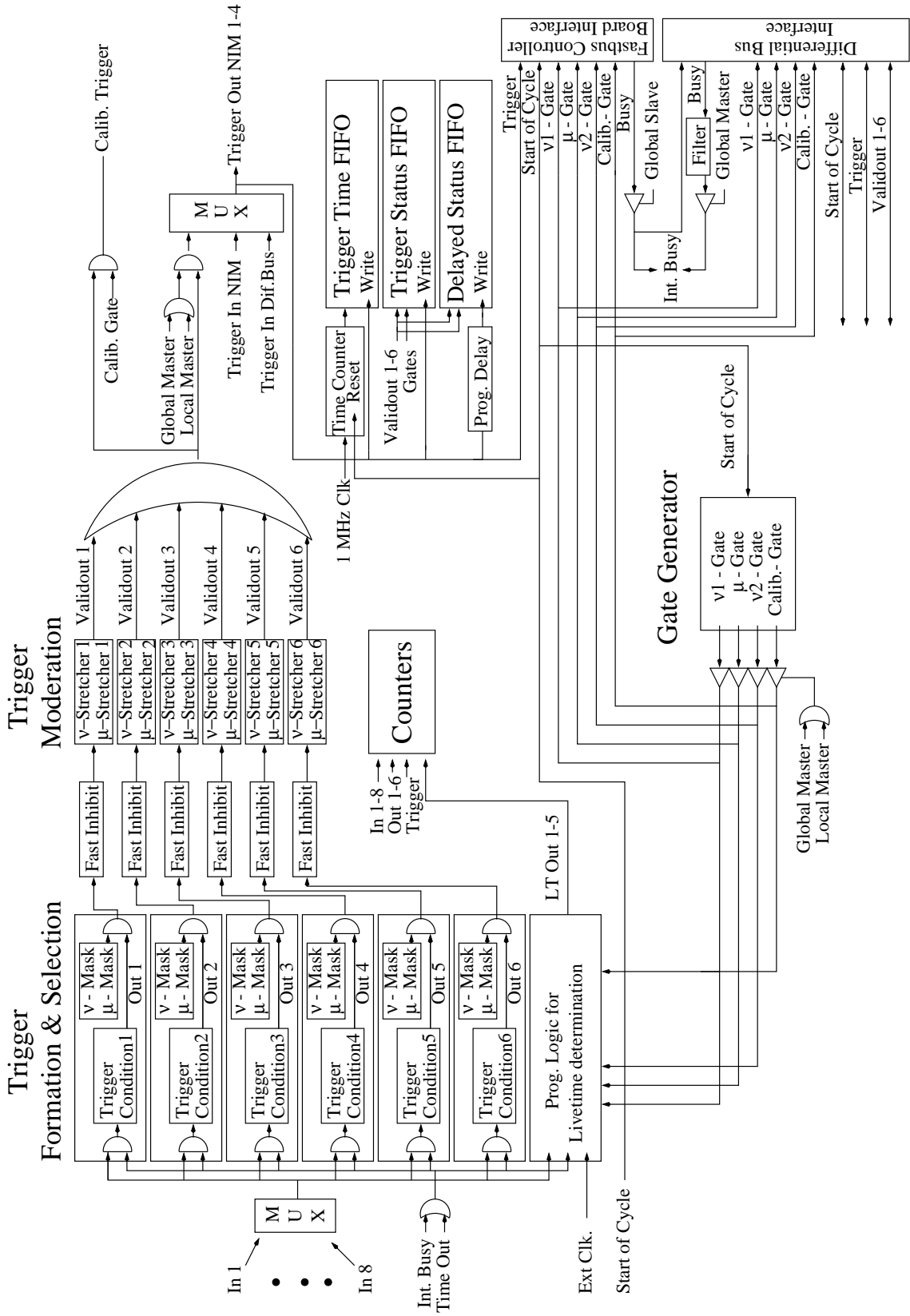
Figure 8: The functionalities of MOTRINO.

5) it is given by:

$$Livetime \ = \ 1 \ - \ \frac{SP5 \ \times (Veto + Trigger + Busy)}{SP5}. \tag{2}$$

4.3.4 FIFO and Counter Information

The rates of the trigger input and output signals as well as the global trigger rate and the coincidence rates for livetime determination are recorded in 16-bit counters for each of the gates. This allows monitoring of the behaviour of the different trigger sources and control of the trigger process.

The time of each trigger relative to the start of the SPS–cycle is stored with a precision of 1 μs in the master and slave modules using a 24-bit FIFO of 2048 words. The time stamp that each trigger receives serves as a control for data integrity and allows monitoring of the width of the neutrino spills. An independent time measurement of the triggers is performed simultaneously with custom built event timer modules in each local system crate.

Two further 16-bit FIFOs record the status of the individual trigger bits. The information is stored as a bit mask, once immediately after a trigger occurred and a second time approximately 200 ns later in order to study trigger correlations in the same event. The counters and FIFOs are read out after each physics gate.

5 Trigger Types and Trigger Efficiencies

In addition to the trigger and the veto scintillators described above, the three calorimetric detectors of NOMAD can also provide fast signals for triggering. The combination of the signals allows the system to trigger on neutrino interactions in different targets. The definition of each trigger together with a discussion of the efficiency for triggering on a given physics process will be given in this section.

5.1 $\overline{\mathbf{V}} \times \mathbf{T_1} \times \mathbf{T_2}$ Trigger

This represents the main NOMAD trigger which allows the study of neutrino interactions in the drift chamber target region. At least one hit in both trigger planes T_1 and T_2 without a hit in the veto counters (V) is required to prevent triggering on through-going muons. The rate for this trigger is $\sim 5.2/10^{13}$ p.o.t. However, only about $0.5/10^{13}$ p.o.t. are potentially interesting candidates for neutrino interactions in the drift chambers. The remaining triggers are due to cosmics rays (about 1.5 per neutrino spill, equivalent to $\sim 1.0/10^{13}$ p.o.t.) outside the acceptance of the veto, non-vetoed muons ($\sim 1.6/10^{13}$ p.o.t.) and neutrino interactions in the magnet coil and flux return yoke ($\sim 2.1/10^{13}$ p.o.t.).

The geometrical acceptance of the two trigger planes for different types of neutrino interactions has been studied in detail with Monte Carlo simulations. Fig. 9 shows a comparison of the geometrical acceptance, which is defined as the fraction of events with tracks crossing both T_1 and T_2, for simulated ν_μ charged current (ν_μ^{CC}) and ν_μ neutral current (ν_μ^{NC}) events as a function of the neutrino energy, track multiplicity and vertex position. The origin of the coordinate

system is placed at the centre of the upstream end of the drift chamber modules (see Fig. 1). The significantly higher acceptance in charged current events is due to the muon from the scattering process, which generally has a higher momentum than particles in the jet from neutral current interactions. The acceptance as a function of the z-coordinate in ν_μ^{NC} events confirms that a fraction of the particles in the jet have a momentum that is too low to reach the second trigger plane.
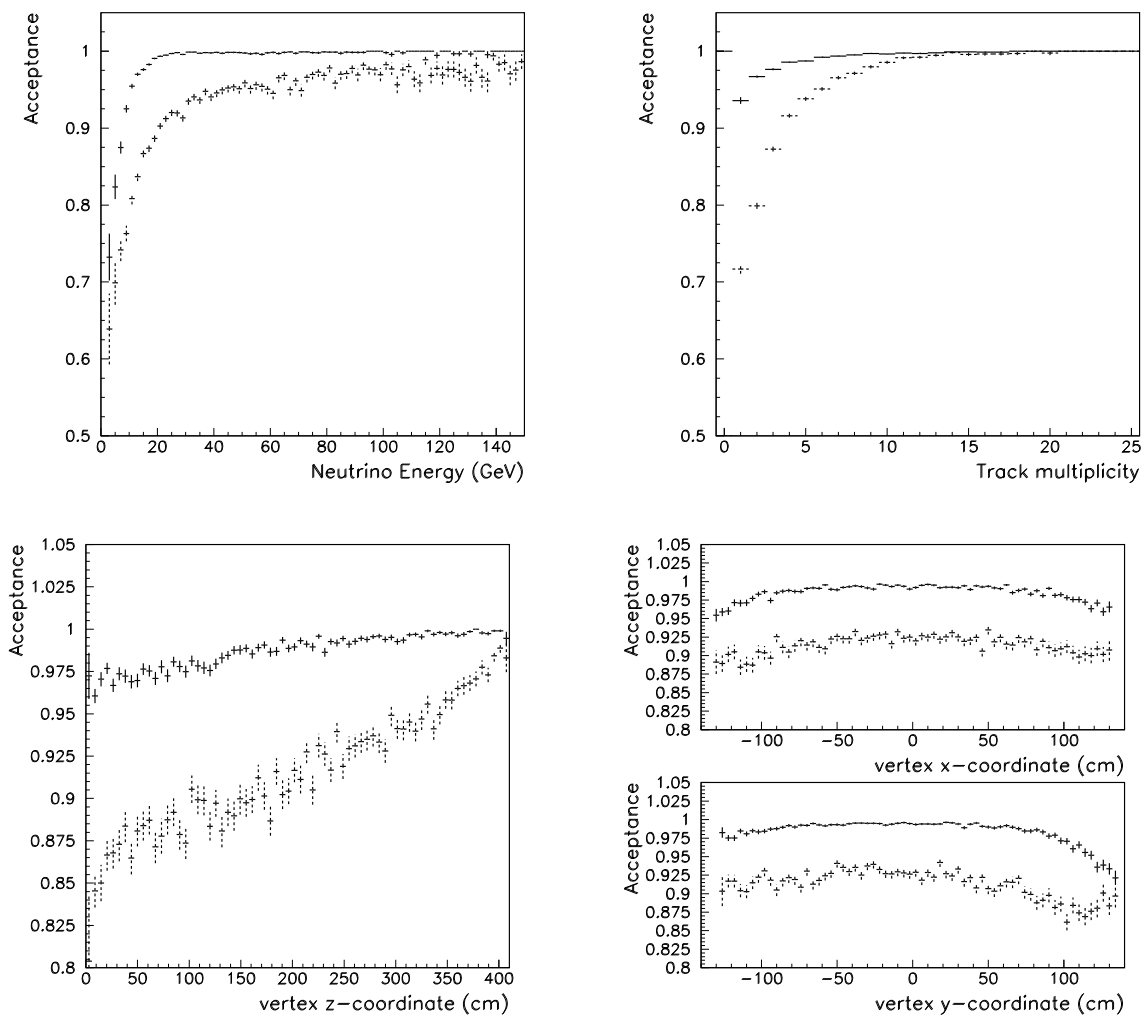

Figure 9: The $T_1 \times T_2$ geometrical acceptance for simulated ν_μ^{CC} (solid lines) and ν_μ^{NC} (dashed lines) events as a function of the neutrino energy, the track multiplicity and the position of the vertex.

Table 2 summarizes the geometrical acceptances for different types of neutrino interactions determined with Monte Carlo simulations, including potential ν_τ oscillation candidates. Since the average energy of ν_e is ~ 15 GeV higher than the average energy of ν_μ , ν_e charged current (ν_e^{CC}) interactions have higher geometrical acceptance than ν_μ^{CC} . Quasielastic-like events and resonances have lower efficiencies than ν_μ^{CC} because the track multiplicity is lower. The acceptance for the leptonic τ-decay channels of ν_τ charged current (ν_τ^{CC}) interactions

15

Interaction type	geometrical acceptance	trigger efficiency
ν_μ^{CC}	$(98.7 \pm 0.1)\%$	$(97.6 \pm 0.1)\%$
ν_μ^{NC}	$(91.7 \pm 0.1)\%$	$(90.7 \pm 0.1)\%$
$\overline{\nu}_\mu^{CC}$	$(97.7 \pm 0.1)\%$	$(95.9 \pm 0.1)\%$
ν_e^{CC}	$(99.5 \pm 0.1)\%$	$(99.1 \pm 0.1)\%$
ν_μ^{CC} $\left(\substack{\text{Quasielastics+}\\\text{Resonances}}\right)$	$(96.8 \pm 0.2)\%$	$(91.0 \pm 0.2)\%$
ν_τ^{CC} $\left(\substack{\text{leptonic } \tau-\\\text{decay channels}}\right)$	$(96.4 \pm 0.2)\%$	$(95.1 \pm 0.2)\%$
ν_τ^{CC} $\left(\substack{\text{hadronic } \tau-\\\text{decay channels}}\right)$	$(97.9 \pm 0.1)\%$	$(97.1 \pm 0.1)\%$

Table 2: Geometrical acceptance and real trigger efficiencies for different types of neutrino interactions in the drift chamber target

is lower than the one for the hadronic decay channels because the momentum of the decay products is lower since there are two neutrinos in the decay.

The trigger efficiencies shown in Table 2 are obtained by weighting the geometrical acceptance by the measured single track efficiencies for T_1, T_2 and the coincidence $T_1 \times T_2$, given in Table 1. Since the average efficiency for a trigger plane with more than one hit is larger than 99.5%, the geometrical acceptance has only to be corrected for the cases of single hits in one or both of the two trigger planes. The trigger efficiency for a given physics process is then given by

$$
\begin{aligned}
\epsilon_{Trig} \times \#Ev. \quad &= \quad \epsilon_{T1} \times \#Ev.(\ Hits_{T1} = 1; Hits_{T2} > 1) \\
&+ \epsilon_{T2} \times \#Ev.(\ Hits_{T1} > 1; Hits_{T2} = 1) \\
&+ \epsilon_{T1 \times T2} \times \#Ev.(\ Hits_{T1} = 1; Hits_{T2} = 1) \\
&+ \#Ev.(\ Hits_{T1} > 1; Hits_{T2} > 1)
\end{aligned}
\tag{3}
$$

A comparison of the geometrical acceptance with the real trigger efficiency shows that quasielastic ν_μ^{CC} interactions are the most affected by the rather low single track efficiency. Note that all neutrino interactions considered have a real trigger efficiency of more than 90%.

The livetime for the $\overline{V} \times T_1 \times T_2$ trigger is $(85.8 \pm 2.8)\%$. It is calculated as given in equation 2 and monitored constantly. The 2.8% width of the livetime distribution is affected by the neutrino beam width, varying from 1-3 ms FWHM, and the proton beam intensity, which varies in the range $(0.8 - 1.3) \times 10^{13}$ p.o.t.

5.2   FCAL Triggers

The front calorimeter (FCAL) of NOMAD is a 17.7 ton iron-scintillator sampling calorimeter which consists of 40 scintillator modules divided into four stacks of 10. The main motivation for this detector is the study of multi-muon physics [22] and searches for neutral heavy particles produced in neutrino interactions. The large mass provides a large sample of these, with two trigger configurations which select quasi-elastic and deep-inelastic neutrino scattering events. The FCAL signal is provided by an active pulse splitter [23] especially designed for this application which provides (i) energy and time output signals for each module and (ii) the analog sum $F_{L,R}^i$ of the left and right hand side of each stack i. A linear fan-in
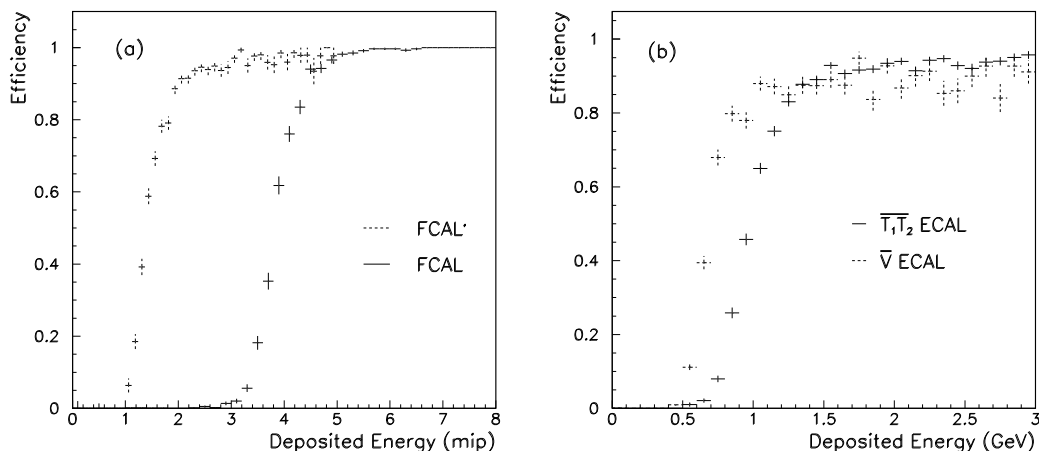
Figure 10: The Efficiency for FCAL(a) and ECAL(b) triggers as a function of the deposited energy

then sums the two signals F_L^i and F_R^i from the left and right side of the same stack. The logical OR of the resulting four signals ($F^i = F_L^i + F_R^i$) is discriminated at a low and a high threshold, corresponding to the two triggers FCAL' and FCAL.

- $\overline{V_8} \times$**FCAL**

  To trigger on deep-inelastic neutrino interactions, the threshold is set at 75 mV. According to Fig. 10 (a), which shows the efficiency of the FCAL trigger as a function of the deposited energy, this corresponds to an energy deposition of 4.0 m.i.p. or ~ 2.0 GeV. Through-going muons are suppressed by the veto subset V_8. About 6.0 neutrino interactions occur in the FCAL for 10^{13} p.o.t. with a negligible background from cosmic muons. The livetime for the $\overline{V_8} \times$ FCAL trigger is $(89.5 \pm 2.2)\%$.

- $\overline{V_8} \times$**FCAL'**$\times$**T$_1$**$\times$**T$_2$**

  This trigger is set up to study quasielastic-like events in the FCAL. Such events allow a relative flux measurement of the neutrino beam as a function of the neutrino energy. For this trigger, a threshold of 15 mV is set, corresponding to an energy deposition between 1.2 m.i.p. and 4.0 m.i.p. (the level at which the previous FCAL trigger is valid), as shown in Fig. 10 (a). Due to this low threshold, the noise rate is higher and the FCAL' signal is therefore used in coincidence with the trigger signals T_1 and T_2. The rate for this trigger is $\sim 1.1/10^{13}$ p.o.t., and its livetime $(89.2 \pm 2.2)\%$.

5.3 ECAL Trigger

The electromagnetic calorimeter (ECAL) is also used as a neutrino target. A range of physics topics can be addressed using events from this trigger, including a search for a new gauge boson in π^0 decays [5] and $\nu_\mu \rightarrow \nu_e$ oscillations [24].

The NOMAD ECAL is composed of 875 lead glass blocks each attached to a tetrode which can operate inside the 0.4 T magnetic field [17]. The tetrode

signals are fed into preamplifiers, followed by shapers composed of three stages. They are arranged in 64 channel modules. Two ECAL triggers were implemented throughout the duration of the experiment:

- $\overline{V} \times$**ECAL**

  The first configuration, used during most of the 1995 run, had the differential output of each of the 64 channels fed to an ECL discriminator with a variable threshold common to each module. The OR of the 64 outputs constitutes the signal for a given module and the wired OR of the 14 modules represents the ECAL trigger signal. Due to the risetime of the shaper, the timing of this signal is dependent on the deposited energy in a lead glass block. However, for energies above 1.5 GeV a time resolution of a few nanoseconds is obtained. The efficiency curve for this trigger, using the veto signal in anticoincidence, is shown in Fig. 10 (b). Because of the time jitter, the veto for this trigger had to be ~ 500 ns long and due to the high $\overline{V}$ rate, the livetime was only $(81.6 \pm 3.5)\%$. The average rate of the $\overline{V} \times$ ECAL trigger is $\sim 2.0/10^{13}$ p.o.t.

- $\overline{T_1 \times T_2} \times$**ECAL**

  During the 1996-1998 data taking periods, the veto signal used for the ECAL trigger was changed to $\overline{T_1 \times T_2}$, to reduce the deadtime associated with $\overline{V}$ being in place. The formation of the ECAL trigger was also modified by imposing that the input to the ECL discriminator be the sum of the 64 analog outputs from the first stage of the shaper. This made the trigger less sensitive to noise and more efficient when a shower is spread over a number of ECAL blocks. The efficiency curve for this new trigger configuration is overlayed on the previous one in Fig. 10 (b). The average threshold is higher, due to the more stringent condition imposed by the sum of the 64 channels, but at higher energies this trigger is more efficient, due to the cases in which the total energy is spread over more than one channel. Also, since the rate of the $\overline{T_1 \times T_2}$ is smaller than $\overline{V}$ the new livetime is higher at $(88.8 \pm 2.3)\%$ and the overall rate is also slightly larger: $\sim 2.5/10^{13}$ p.o.t.

5.4 STAR Trigger

For the 1997 and 1998 runs, a target consisting of 45 kg of boron carbide plates interleaved with silicon detectors covering an area of 1.14 m^2 was installed inside the NOMAD magnet replacing the first three drift chambers [25]. The aim of this Silicon TARget (STAR) is to study the vertex and impact parameter resolution of neutrino interactions measured with silicon detectors. The trigger of this sub-detector consists of the logic condition $\overline{V_8} \times \overline{V_S} \times T_S \times T_1$, where $\overline{V_S}$ is the logical OR of signals from two scintillators in front of the target in anticoincidence, T_S is the OR from two scintillators downstream of the target, $\overline{V_8}$ is the signal from the central NOMAD veto also in anticoincidence and T_1 is the signal from the first of the NOMAD trigger planes. A special busy logic formed in a dedicated module is used for the STAR trigger because the time taken to perform a valid readout of the 32,000 silicon channels is rather long (~ 3 ms). The rate of this trigger is $(0.33 \pm 0.07)/10^{13}$ p.o.t. and the livetime is $(59 \pm 5)\%$.
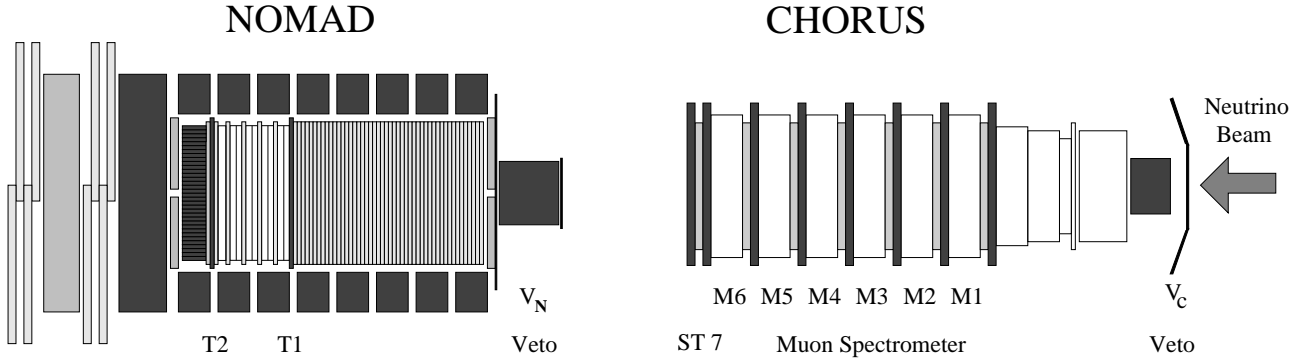
Figure 11: Setup of the CHORUS-NOMAD neutral heavy particle trigger

5.5 CHORUS–NOMAD Trigger

Motivated by a search for neutral heavy particles [26] a joint trigger with the CHORUS experiment was set up in 1996 [27]. Both experiments record events in the case of simultaneous interactions in the CHORUS muon spectrometer and the NOMAD drift chamber target. Such a configuration corresponds to the signature of a hypothetical neutral heavy particle (NHP) produced in CHORUS and decaying in NOMAD. Fig. 11 shows the position of the various subdetectors used for the formation of this trigger. The trigger condition is:

$$NHP_{Trig} \; = \; \overline{V_C} \times \left(\sum_{i=1}^{6} M_i \right) \times \overline{ST_7} \times \overline{V_N} \times T_1 \times T_2$$

On the NOMAD side, the events which satisfy this condition are a subset of the $\overline{V} \times T_1 \times T_2$ triggers. In addition to the veto counters of the two experiments, plane 7 of the streamer tubes in CHORUS is used to suppress beam muons and charged current interactions in the muon spectrometer.

5.6 Random Trigger

A Random trigger has also been implemented inside MOTRINO in order to study detector occupancy, mainly associated with out-of-time muons from the neutrino beam. A signal 22 μs after every 16th valid neutrino trigger, the delay equivalent to one turn of the protons around the SPS, is chosen to guarantee coincidence with a proton extraction which could cause out-of-time muons and background neutrino interactions in NOMAD. The prescaling factor ensures that approximately one trigger per neutrino spill is recorded.

5.7 Muon Triggers

In addition to the triggers in the neutrino spills, various other triggers are set up during the muon gate. These triggers are used for alignment and calibration purposes and their rate can be moderated using the stretchers of MOTRINO. The buffer size of the front-end electronics allows a maximum of 256 triggers but on average 15 neutrino and 20 muon spill triggers (from a total of 60 selected) are written to tape. Their description is as follows:

- **$V \times T_1 \times T_2$**

  Sensitive to through-going tracks in the full fiducial area of NOMAD this trigger is used for drift chamber alignment and the calibration of different subdetectors with minimum ionizing particles.

- **$V_8 \times T_1 \times T_2 \times FCAL'$**

  This trigger was implemented to enhance the sample of muons crossing FCAL and other portions of the detector that are not selected by the previous trigger due to the muon beams crossing the detector at an angle with respect to the neutrino beam direction.

- **$V_8 \times T_1$ and $V_8 \times T_2$**

  These triggers were implemented for the measurement of the efficiency of T_2 and T_1 respectively.

- **$V \times T_1 \times T_2 \times ECAL \times (\overline{HCAL})$**

  This trigger allows selection and study of electrons from muon decay or delta rays. The OR from the signals of the NOMAD hadronic calorimeter (HCAL) [3] is placed in anti-coincidence to exclude triggering on muons in the case that muon decay signals are chosen. The HCAL condition is not included in the trigger when delta rays are required.

- **$V_8 \times V_S \times T_S \times T_1$**

  This is a trigger that selects muons crossing the silicon target STAR for alignment and calibration purposes.

6 Conclusion

The trigger for the NOMAD experiment consists of large area plastic scintillators which serve as a veto upstream of the main NOMAD target, two planes of trigger scintillators operating inside the 0.4 T magnetic field in which proximity mesh photomultiplier tubes have been used, and custom-built programmable VME modules (MOTRINO) which take care of all the trigger logic decisions, signal synchronisation, gate generation, event counting and livetime calculations for the experiment.

The efficiencies for all the NOMAD physics triggers have been found to be greater than 90%, with livetimes for the triggers varying between 84% and 90%, depending on the trigger, the beam intensity and the narrowness of the neutrino spill. The flexibility of the NOMAD trigger has enabled NOMAD to enhance its physics potential beyond the study of $\nu_\mu \rightarrow \nu_\tau$ oscillations.

7 Acknowledgements

References

[1] NOMAD Collaboration, J. Altegoer *et al.*, Physics Letters **B 431** (1998) 219.

[2] J.J. Gómez-Cadenas, *Recent Results from the NOMAD Experiment*, XVIIIth International Conference on Neutrino Physics and Astrophysics, Takayama, Japan (June 1998); D. Autiero, *Results from the NOMAD Experiment*, XXIX International Conference on High Energy Physics, Vancouver, Canada (July 1998).

[3] NOMAD Collaboration, J. Altegoer *et al.*, Nucl. Instr. and Meth. **A 404** (1998), 96.

[4] E. Pennacchio, Nucl. Phys. **B 65** (Proc. Suppl.) (1998), 177; B. Schmidt, *Recent results from the NOMAD experiment*, Proc. of the XXV SLAC Summer Institute Topical Conference on the "Physics of Leptons", Stanford, 1997; M. Mezzetto, Nucl. Phys. **B 70** (Proc. Suppl.) (1999), 214.

[5] NOMAD Collaboration, J. Altegoer *et al.*, Physics Letters **B 428** (1998), 197.

[6] The scintillation counters were used previously by a group from Padova University in the $n\overline{n}$ experiment at I.L.L. Grenoble: M. Baldo Ceolin *et al.*, Nuovo Cimento A 105 (1992), 1679; M. Baldo-Ceolin *et al.*, Zeit. für Phys. **C 63** (1994), 409.

[7] A. Cavestro *et al.*, Nucl. Instr. and Meth. **A 305** (1991), 488.

[8] LabVIEW User Manual for SUN, September 1994 Edition (Austin, TX, National Instruments Corporation, 1992, 1994).

[9] The CHORUS Collaboration, E. Eskut *et al.*, Nucl. Instr. and Meth. **A 401** (1997), 7.

[10] BICRON Corporation, data sheet for Premium Plastic Scintillators BC-408.

[11] J. Altegoer, *Untersuchung der Szintillationszähler für den Trigger des NOMAD-Experiments mit Myonen aus der Kosmischen Höhenstrahlung*, Diploma Thesis, Dortmund (1994).

[12] F. Takasaki, K. Ogawa and K. Tobimatsu, Nucl. Instr. and Meth. **228**, (1985), 369.

[13] S. Suzuki *et al.*, *New Mesh PMTs for High Magnetic Environments*, HAMA-MATSU Photonics K.K., Ichino-cho, Japan, 1987.

[14] HAMAMATSU Photonics, data sheet R-2490-05 (1991).

[15] L.S. Peak and P. Soler, Nucl. Instr. and Meth. **A 301** (1991), 341.

[16] G. Finsel *et al.*, Nucl. Instr. and Meth. **A 290**, (1990), 450.

[17] D. Autiero *et al.*, Nucl. Instr. and Meth. **A 373**, (1996), 358.

[18] The H1 SpaCal Group, R.-D. Appuhn *et al.*, *Series Tests of Fine Mesh Photomultiplier Tubes in Magnetic Fields of up to 1.2 Tesla*, DESY 97-070 (April, 1997).

[19] B. Schmidt, *Study of ν_μ Charged Current Interactions and Search for $\nu_\mu \leftrightarrow \nu_\tau$ Oscillations in the Channel $\tau^- \to \mu^- \overline{\nu}_\mu \nu_\tau$ with the NOMAD Detector at the CERN Wideband Neutrino Beam*, Doctoral Thesis, Dortmund (1997).

[20] GAL Data Book, Lattice Product Catalogue, Hilsboro (1992).

[21] ALTERA Data Book, San Jose (1995).

[22] S.B. Boyd, *A Measurement of the charm quark mass to Next-To-Leading order using dimuon events in the NOMAD detector*, PhD Thesis, The University of Sydney (1998).

[23] D. Geppert, *Bau von Komponenten eines Scintillator-Hadron-Kalorimeters und dessen Kalibrierung im NOMAD-Experiment*, Diploma Thesis, Dortmund (1995).

[24] Th. Weiße, *Comparison of Muonic and Electronic Final States in the NOMAD Experiment at the CERN Wide-band Neutrino Beam*, Doctoral Thesis, Dortmund (1997).

[25] G. Barichello *et al.*, Nucl. Instr. and Meth. **A 419**, (1998), 1-15.

[26] P. de Barbaro, *Search for Neutral Heavy Leptons in Neutrino-Nucleon Interactions at the FNAL Tevatron*, Doctoral Thesis, University of Rochester (1990).

[27] M.G. van Beuzekom *et al.*, *The Trigger System of the CHORUS Experiment*, CERN-EP/98-131 (1998).